High velocity outflows along the axis of pulsed power driven rod z-pinches

Cite as: AIP Advances **10**, 105009 (2020); https://doi.org/10.1063/5.0019843
Submitted: 12 August 2020 • Accepted: 16 September 2020 • Published Online: 05 October 2020

D. Yanuka, S. Theocharous, J. P. Chittenden, et al.

High velocity outflows along the axis of pulsed power driven rod z-pinches

Cite as: AIP Advances 10, 105009 (2020); doi: 10.1063/5.0019843
Submitted: 12 August 2020 • Accepted: 16 September 2020 •
Published Online: 5 October 2020

D. Yanuka, S. Theocharous,[a] J. P. Chittenden, and S. N. Bland

AFFILIATIONS

Plasma Physics Group, Imperial College London, London SW7 2BW, United Kingdom

[a]Author to whom correspondence should be addressed: savva.theocharous12@imperial.ac.uk

ABSTRACT

We report on initial observations of high velocity outflows from the ends of a rod compressed using pulsed power. 1 mm and 2 mm diameter copper rods were placed in a water bath and driven by ~0.6 MA currents with rise times of ~700 ns. Laser backlit framing images and streak photography showed an outflow of the material from the ends of each rod, of the initial velocity of up to 7 km/s, which began ~500 ns after the start of the current pulse and continued throughout the experiment. Ballistics gel was used to help separate low density gas/plasma from any solid/liquid component in the outflow, successfully capturing the material from larger diameter rods (enabling an estimate of its energy) and tracing the path of the material that passed straight through the gel with smaller rods. Experimental results were compared to 1D and 2D MHD simulations performed with the Gorgon code. These suggested that the outflow had two different components, resulting from two different physical processes. Differences in the resistivity between the copper rod and stainless steel anode result in the opening of a small gap between them and ablated stainless steel being projected above the rod, which is captured in framing and streak images. Later in time, a dense copper material, pinched by the magnetic pressure, is launched—explaining the ballistics gel results. The simulations also suggest that the tamped explosion of the rod surface plays a small role in any outflow.

I. INTRODUCTION

The use of pulsed power to drive high pressure conditions for Equation of State (EOS) research has rapidly increased over the last two decades. In planar geometries, the high currents and excellent pulse shaping capabilities of the Z accelerator have enabled quasi-isentropic pressures of ~500 GPa to be attained with large multi-mm^2 target areas, giving unprecedented experimental accuracies to these measurements.[1,2] In order to obtain higher pressures, researchers have explored employing convergence, driving cylindrical liners with reliable axial uniformity instead of planar configurations. In the latest experiments, ~1 TPa pressures have been obtained in magnetically compressed liners made of Ta, Cu, and Al.[3] Here, a set of optical probes on the inside surface of the liner wall enable its macroscopic properties of pressure and density to be mapped as the liner is compressed by the magnetic pressure.

A natural extension of this technique is to use the liner to compress a filler material. The Magnetized Liner Inertial Fusion (MagLIF) concept at Sandia uses such a system—compressing a magnetized, hot D-T plasma to fusion conditions;[4] so, understanding the implosion of these filled liners is critically important. For EOS research, the liner implosion is relatively slow and the fill cold[5,6]—hence, the compression of a solid metallic rod could even be considered.

We can explore the scaling of a convergent, magnetically driven rod using a simple Mie Grüneisen EOS,[7]

$$U = \left(\frac{P+K}{\Gamma}\right)V, \tag{1}$$

where K is the bulk modulus, Γ is the Grüneisen parameter, and U, P, and V are specific internal energy, pressure, and specific volume, respectively.

Assuming K and Γ are both constant, the relationship between P and V for an isentropically compressed sample can be found,[7]

$$P = \frac{K}{\Gamma+1}\left[\left(\frac{V_0}{V}\right)^{\Gamma+1} - 1\right], \tag{2}$$

where V_0 is the initial specific volume. Providing the field does not diffuse into the rod, the magnetic pressure is

$$P = \frac{\mu_0 I^2}{8\pi^2 r^2}. \quad (3)$$

Assuming equilibrium, we can equate (2) and (3) and substitute $V = V_0 (r/r_0)^2$ for a rod to solve for r and calculate pressure. A small, university scale generator might have a rise time of 500 ns and a current of ~1 MA. Using this peak current with Eqs. (2) and (3), we might expect an initially 1 mm diameter copper rod to be compressed to a diameter of ~0.8 mm and attain a pressure of ~90 GPa. For comparison, in planar geometries, to prevent issues with lateral waves affecting the target, pressures would typically be limited to 1 GPa–10 GPa.

Current diffusion into small diameter rods, however, could significantly affect the results of such experiments. As the material is heated on the outside of the rod, current will diffuse inward, which will alter the amount of material being compressed. If current diffuses far enough into the rod, it will also heat the material on axis. Based on the calculations of non-linear magnetic diffusion in Ref. 8 and assuming that a generator has a sine wave like current with 500 ns rise time, we might expect diffusion to reach a diameter of ~350 μm for a 1 mm rod, suggesting the material on axis could remain relatively cold.

Of course, to explore these high pressures and non-linear diffusion effects in detail, we should employ resistive magnetohydrodynamic (MHD) simulations with a tabulated EOS. The simple calculations, though, suggest that utilizing a rod could be a very effective way to attain extreme pressures. On a larger pulsed power facility, such experiments may be the best way to exploit the electrical energy available. Experiments on a university scale generator, meanwhile, could also provide important information on power flow at high current densities, including plasma formation around the rod and its connections, and the rate of current diffusion into the rod.[9]

One of the issues facing rod experiments is the difficulty in diagnosing the conditions created internal to the rod. On the Z facility, the x-ray radiography system operates at ~6 keV, limiting measurements to very low Z materials like beryllium. At Imperial College, we are developing hard x-ray radiographic systems based around X-pinch sources[10] to probe higher Z materials, but while these are being perfected, we are also exploring how the outflow from the end of a rod could be used to diagnose internal conditions and possibly drive separate high pressure experiments. Given the relatively long duration of pulsed power experiments (100s–1000s of ns), as the rod is compressed radially, the pressure in the rod is free to release at its end faces. An experiment can be designed in which the end electrodes are connected radially around either end of the rod, such that diagnostic access to the end faces of the rod is possible. Of course, in such a setup, the electrodes connecting to the rod must have a reasonable thickness to maintain low resistance, so the rod material adjacent to the electrodes in the rod may experience less current and so remain relatively uncompressed—these "end effects" could affect the outflow. Given the complexity in modeling such a system—requiring a mix of 2/3D resistive MHD modeling in condensed materials—any experimental information on the outflow of a rod would be useful and could enable theory to then optimize the design of a rod experiment producing a uniform pressure drive across the face of the rod.

In this paper, we describe initial experiments utilizing the MACH (Mega Ampere Compression and Hydrodynamics) pulsed power facility at Imperial College London to study the outflows of material from different diameter copper rods driven by currents of ~0.6 MA. To prevent any issue with electrical breakdown along the rods, each was submerged in a bath of deionized water, with only the flat ends of the rod exposed (to air). The water bath also tamped any radial expansion of the surface of the rod, and so, it could provide an additional source of pressure in the experiments, which was explored through simulation.

The rest of the paper is structured as follows. In Sec. II, we describe the experimental setup and diagnostics. Laser shadowgraphy imaging, supplemented by streak photography in the axial direction, is used to study early dynamics of the outflows. In some shots, ballistics gel was placed on top of the rod to help separate any low density gas/plasma outflow from solid/liquid components. In Sec. III, we present our results and comparisons to simple calculations, while in Sec. IV, 1 and 2D MHD simulation using the Gorgon code are used to explore the dynamics of the rod. Finally, in Sec. V, we summarize our results and present future research directions.

II. EXPERIMENTAL SETUP

MACH is a compact pulsed power generator that was designed to produce up to 2 MA currents with ~450 ns rise times when connected to a low inductance (<5 nH) transmission line and load. It is configured as a set of 40 parallel capacitors in series with 20 low inductance switches that are connected via a radial feed. In its simplest form, this can be represented as a lumped 6 μF capacitance in series with an inductance of ~20 nH and a resistance of 15 mΩ measured to the end of the transmission line.

For these experiments, the capacitors in MACH were discharged through 1 mm and 2 mm copper rods of 32 mm length immersed in deionized water. 60 kV charging voltages were used, to reduce any detrimental effects caused by reversals on the capacitor lifetime. The current through the rods was measured using four Rogowski coils, one on each side of the generator, and the voltage across the rods was measured using two D-Dot probes placed 90° apart from each other and at 15 cm from the center.

A schematic of the internal part of the generator where the rod is inserted is presented in Fig. 1. There is air above and below this setup. The rods were inserted through holes in the bottom and top electrodes as shown in Fig. 1 at a depth of 1 mm on each side so that the length of the rod in between the electrodes was 30 mm. The resistance and inductance (including the electrodes connected to the transmission line) for the 1 mm rod are calculated to be 0.57 mΩ and 20.9 nH, respectively, and those for the 2 mm rod are 0.14 mΩ and 17.3 nH, respectively.

To diagnose the outflow, two separate methods were used. The first method included a fast framing camera and a streak camera capturing shadowgraph images of the outflow backlit by a 6.5 W, 532 nm continuous laser (in the direction shown in Fig. 1). The framing camera provided 12 independently timed frames of ~5 ns exposure with a 9.3 mm field of view. The streak camera was arranged to image in the axial direction along ~9 mm from the face of the rod.

In the second method, ballistics gel was used to help separate any different components in the outflow. Any low density

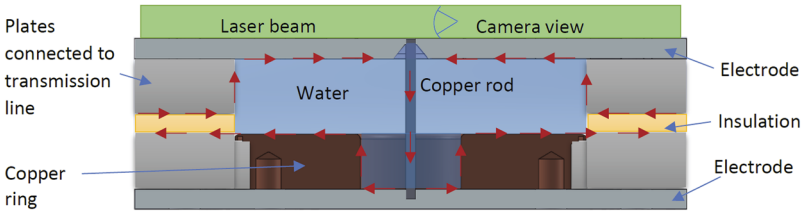

FIG. 1. Schematic of the rod experiment setup. The red arrows indicate the current flow.

gas/plasma tends not to penetrate ballistics gel and instead just affects the surface. A high density condensed material, however, will penetrate the gel or even pass through it. In our experiments, the ballistics gel blocks were placed either straight on top of the rod or at a distance of 158 mm from the top of the rod. The gel's density was found to be ~915 kg/m^3, and the block thickness was in the range of 11 cm–45 cm (with the possibility of stacking several blocks together). Pre-shot pictures of the latter case are shown in Fig. 2.

III. EXPERIMENTAL RESULTS AND ANALYSIS

A. Electrical characteristics

Typical experimental current waveforms for the two rod diameters are presented in Fig. 3(a) and show a decaying oscillatory structure, as expected from a RLC series circuit. If the inductance/resistance of each rod had remained constant over the experiment, we would have expected the waveforms to be similar to those predicted by the circuit model shown in Fig. 3(b). Here, the slightly lower inductance of the 2 mm rod means that the current waveform has a shorter rise time and smaller oscillation period; though as the difference in inductance between the rods is relatively small compared to the inductance of the transmission line and generator, the difference in period is also small. The circuit model, however, does not account for diffusion of current into the rod as the experiment progresses or changes in resistance during the experiment as a result of heating of the rod material.

In the experiment, we observe the current waveforms from the 1 mm and 2 mm rods to initially overlay, and the rate of rise of current through each is then comparable to the circuit model. However, from ~600 ns, as the current flowing through each rod reaches its peak, the experimental results start to diverge from the model and from each other. The period of the current flowing through the 2 mm rod starts to slowly decrease compared to the model, completing one period of oscillation at 2.95 μs compared to 3.4 μs. Surprisingly the initially higher inductance 1 mm rod develops an even faster oscillation, with one period completing at 2.4 μs. The current flowing through the 1 mm rod also decays much faster than that of the 2 mm rod.

The faster decay rate suggests that from approximately peak current, current through the 1 mm rod is passing through a more resistive material than the 2 mm case, while the change in period suggests that the mean radius that current is flowing through is larger than in the 2 mm case, reducing its relative inductance. This is consistent with the results of 1D MHD simulations of the material in the rods discussed in Sec. IV.

B. Shadowgraphy results

Images from the framing camera are shown in Figs. 4 and 5 for the 2 mm and 1 mm rods, respectively. Both show an outflow of the material starting from ~0.5 μs after the start of the current pulse. The outflow expands both radially and axially from the same radius as the rod. The images each appear to show two parts of the outflow—a

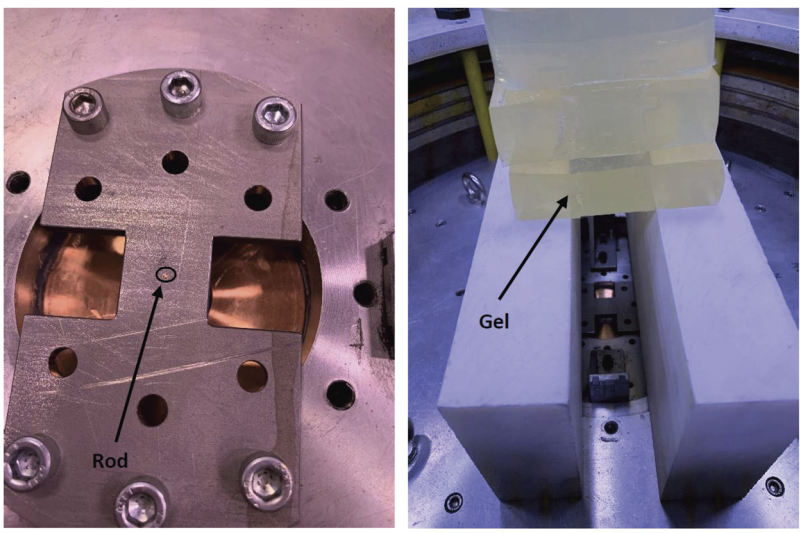

FIG. 2. Pre-shot pictures of a 1 mm rod experiment and placement of ballistics gel.

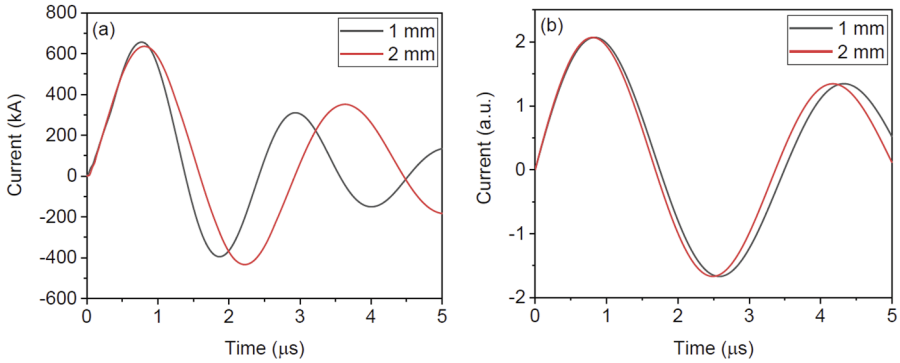

FIG. 3. Current flowing through the 1 mm and 2 mm diameter rods (a) measured in experiment and (b) predicted by the circuit model with constant values of inductance and resistance.

low opacity cocoon, with a much darker central region. The cocoon moves at the same radial and axial velocity as the denser region, and its spacing is consistent with it being a shock wave in the air caused by the rapidly expanding material.

A plot of the axial position of the outflow (from the dark region) and its velocity are presented in Fig. 6 along with data taken via the streak camera. The initial velocity of the outflow from the 1 mm rod is significantly higher than the 2 mm rod, 7 km/s vs 4 km/s though the velocity of both rapidly falls to ~2 km/s by ~2 μs after the start of the current. It should be noted that attempts were made to diagnose the velocity of the outflowing material using a multi-point photon Doppler velocimetry[11] system. This would have allowed velocity to be measured with much higher temporal resolution, as well as provide multiple velocity traces along the diameter (with spatial resolution 250 μm), which could help to clarify the origin of the outflow. However, the velocity was not detected by the diagnostic due to insufficient reflection of the target beam. This is likely because the outflow was a dense gas/plasma, and only a very small part of the light was reflected/scattered back to the fiber probe while the majority was absorbed or refracted out of the system. This effect would be worsened by the non-uniform structure of the outflow, as is visible in the shadowgraphy images.

If the outflow we observe in the images is due to the majority of the rod material being projected upward, we can derive an order of magnitude estimate of the maximum pressure generated inside the rod,

$$PA = m\frac{dv}{dt}\cdot\frac{dx}{dx} \rightarrow PA = mv\frac{dv}{dx}$$
$$\rightarrow A\int Pdx = m\int vdv \rightarrow \bar{P} = \frac{mv^2}{2AL}, \quad (4)$$

where P is the pressure, $\bar{P}$ is the average pressure inside the rod, and L is the length of half a rod. Taking $m \sim 6.76 \times 10^{-5}$ kg to be the mass of half of a 1 mm diameter rod, and taking the experimentally

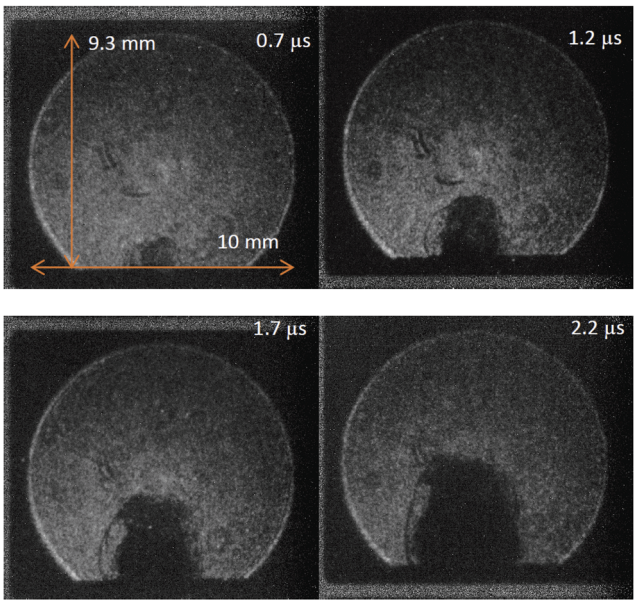

FIG. 4. Rod outflow—2 mm.

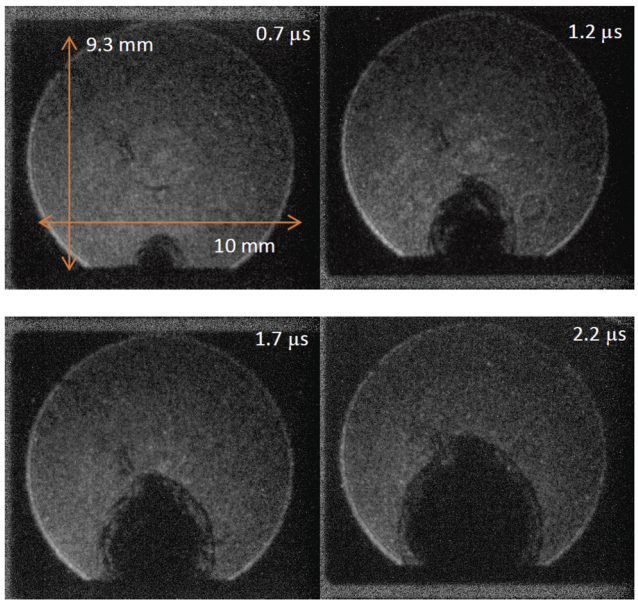

FIG. 5. Rod outflow—1 mm.

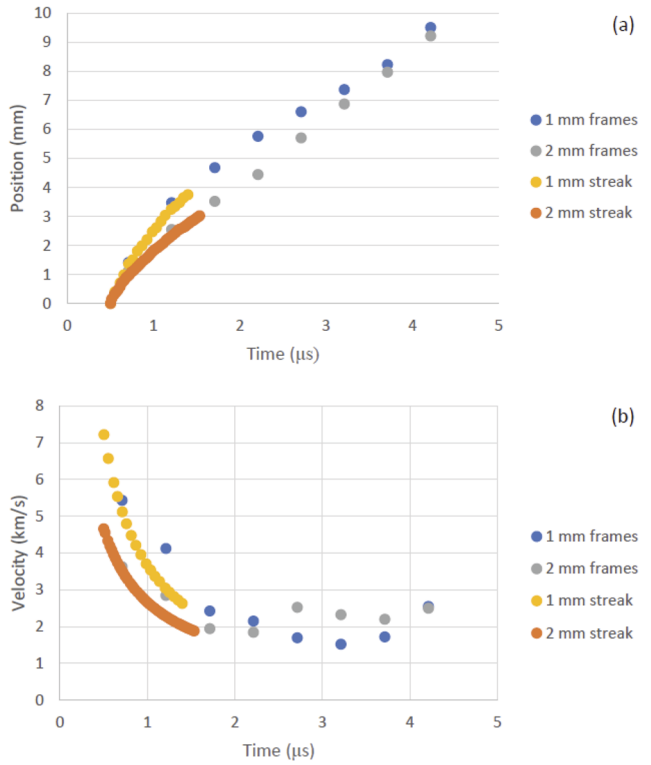

FIG. 6. Outflow (a) positions and (b) velocities from framing and streak image results.

found maximum velocity of 7000 m/s, we get an average pressure of $\bar{P} \approx 220$ GPa, while a similar calculation for the 2 mm rod with a velocity of 5000 m/s gives $\bar{P} \approx 112$ GPa. The validity of such a calculation, though, is limited—for instance, it assumes that all of the material of the rod is accelerated instantaneously to either one of the two ends (leaving a non-physical vacuum behind). It also does not take into account the compressibility of copper; however, at pressures of up to 300 GPa, the shock compression path corresponds to a compression ratio ρ/ρ_0 of <1.5,[12] indicating that compression of the metal does not have a significant effect in this regime. Although the compression ratio increases with pressure beyond this, if the pressures attained were high enough (on a higher current experiment), it could potentially become partially degenerate as described in Ref. 5.

Such simple calculations and assumptions also cannot easily explain the shape of the outflow that is seen. While the axial velocity of the outflow starts high then slows down to ~2000 m/s for both 1 mm and 2 mm diameter rods, the radial velocity strongly depends on where in the outflow it is measured. Taking the maximum radius of the outflow, the velocity is initially ~3.5 km/s for the 1 mm rod and ~2.5 km/s for the 2 mm rod before rapidly decreasing; however, the outflow has a distinct bubble shape—narrowing at the tip and base. A simple release of a high pressure material might be expected to have an ever increasing outflow diameter, as the material freely expands.

C. Ballistics gel results

To explore the composition of the outflow from the face of the rod, we utilized ballistics gel blocks as a trapping medium. Using a gel block placed directly on top of either the 1 mm or 2 mm diameter rod resulted in a ~10 mm area of blackened, melted gel on the face of the block adjacent to the rod [Fig. 7(a)]. Although no entrance hole could be seen within this blackened area, the rear surface of the block displayed a ~1 mm exit hole, directly opposite the area [Fig. 7(b)]—a distance of ~40 mm through the gel. This is consistent with the outflow from the rod having two parts—a cloud of hot plasma/gas expanding from the rod or around the rod accompanied by a condensed projectile.

In subsequent shots, the ballistics gel block was spaced ~158 mm from the 1 mm rod, enabling any expanding gas/plasma to dissipate before reaching the gel. An entrance hole of ~1.5 mm to 2 mm diameter was then observed. A small, ~2 mm^3 solid piece of copper was caught at a distance of 5.25 cm inside the gel. In this case, we presume that the piece of copper was slowed by the air as it left rod, potentially through tumbling. We can use the depth the copper penetrated into the ballistics gel to estimate the energy in the projectile when it entered the block. Copper needs to overcome the tensile strength of the gel σ, and then, the energy lost in the process

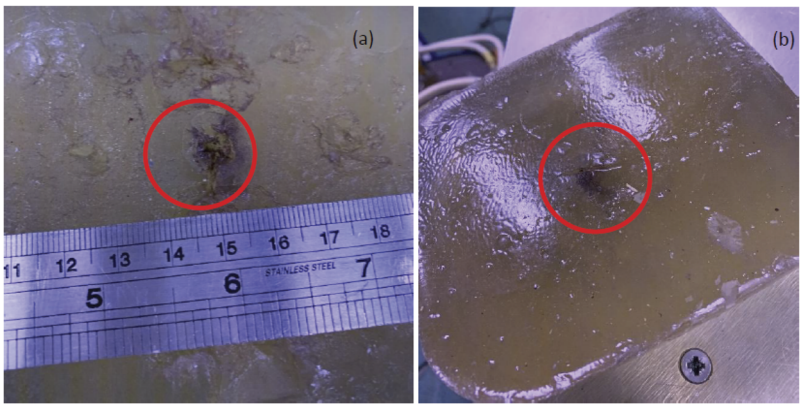

FIG. 7. (a) Outflow trace in ballistics gel positioned directly on top of the rod (the side shown was facing down) and (b) hole in the upper side of the gel when put right on top shows the exit of projectile (the side shown was facing up).

of penetration is

$$dE = \sigma A dx \rightarrow E = x_p A \sigma, \quad (5)$$

where dx is an infinitesimal step inside the gel and x_p is the penetration distance. We estimate σ = 10 MPa, which is an average value for an elastic polymer like ballistics gel.[13] With this estimate, the energy lost due to the tensile strength of the gel is $E \approx 0.6$ J. However, in capture experiments, a better estimate of the energy of a projectile is obtained by considering the viscous drag on it. Here, we assume the projectile penetrates a fluid and use the drag equation $F_d = 0.5 C_d A \rho v^2$,[14] where F_d is the frag force, C_d is the drag coefficient, A is the projectile front area, ρ is the gel's density, and v is the projectile's velocity. The infinitesimal energy then lost every step is

$$dE = -\frac{1}{2} C_d A \rho v^2 dx = -\frac{E}{m} C_d A \rho dx \rightarrow E(x) = E_0 e^{-\frac{C_d A \rho}{m} x}. \quad (6)$$

The value of the drag coefficient is usually obtained experimentally and depends on the projectile's shape and several dimensionless parameters, such as the Reynolds and Mach numbers. With the approximation that the projectile in this experiment is a small sphere or cube, the values of the drag coefficient vary roughly between 0.5 and 1.5,[14] so it was taken in this calculation to be 1. Inserting all these values to Eq. (6), we find that the energy that is "left" after the projectile stopped is $E \sim 1$ J, which is very close to the energy lost due to the tensile strength. Of course, the drag coefficient could be much higher, especially as the projectile may have been tumbling as it entered the gel. In either case though, the energy is very low in comparison to the stored energy in MACH (10.8 kJ) and does not represent a large fraction of the rod mass moving at multi-km s^{-1} (~100s of J).

IV. MAGNETOHYDRODYNAMIC SIMULATIONS

In order to obtain a better understanding of the dynamics of the rods as they were compressed, 1D radial simulations were performed using the GORGON resistive MHD code.[15,16] The simulations used a Lee–More–Desjarlais conductivity model[17] and a Johnson–Cook elastic–plastic material strength model for copper.[18] The equation of state data for both copper and water were calculated using the Frankfurt Equation of State (FEoS) model.[19] The spatial resolution of these simulations was 2.5 μm, to allow the internal dynamics of the rods to be resolved. A $\sin^2$ current waveform with the same peak current and rise time as observed for each rod was used to drive the simulations.

Line outs of the thermal pressure, density, electron temperature, and current density from simulations with a 2 mm rod are shown in Fig. 8, and those from a 1 mm rod in Fig. 9. In the case of the 2 mm rod, the material in the entire rod remains below the boiling point while the current increases, and it only starts to boil and expand from the surface of the rod at ~800 ns. At the start of the current pulse, current diffuses into the outer radius of the copper rod and starts to heat it ohmically. As its resistance increases, likely due to melting, current and field diffuse inward with the peak of the current density remaining in metallic copper with a lower current density tailing off through the heated material toward the outside of the rod. Magnetic pressure, which has a leading edge determined by current diffusion, results in a compression wave heading toward the axis of the rod. This wave travels faster than the current diffusion. On axis, the pressure continues to build in cold material (before any ohmic heating has occurred in this region) reaching a peak ~11 GPa between 700 ns and 800 ns. For comparison, the simple Mie Grüneisen model described in Eq. (3) predicts pressures of

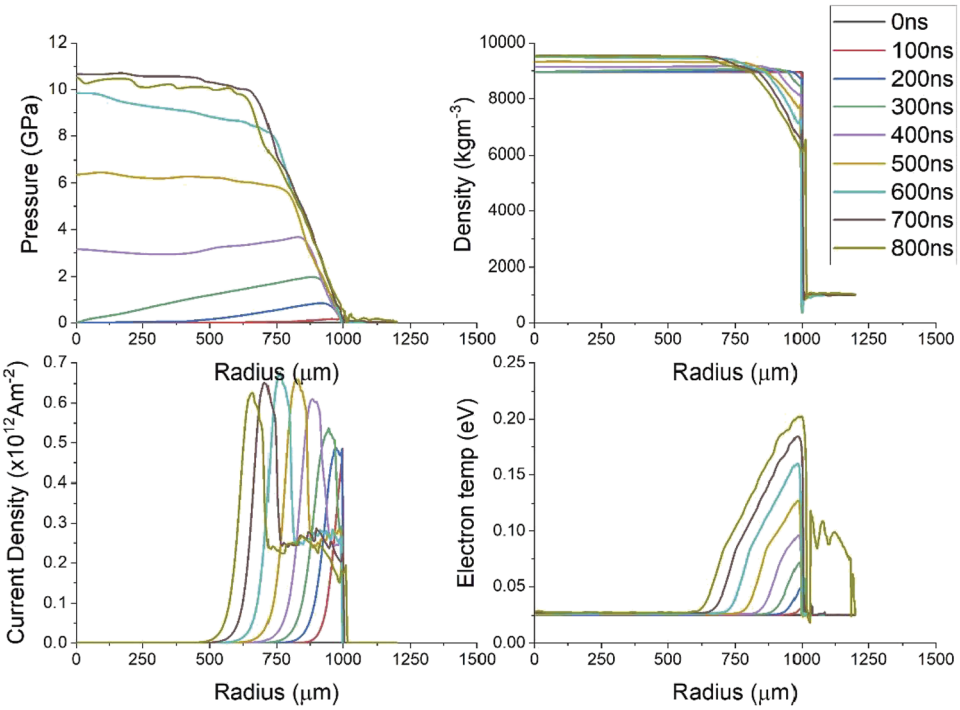

FIG. 8. Line outs of the thermal pressure, density, current density, and electron temperature from simulations for a 2 mm Cu rod driven by 0.63 MA current peaking at 800 ns (matched to experiment).

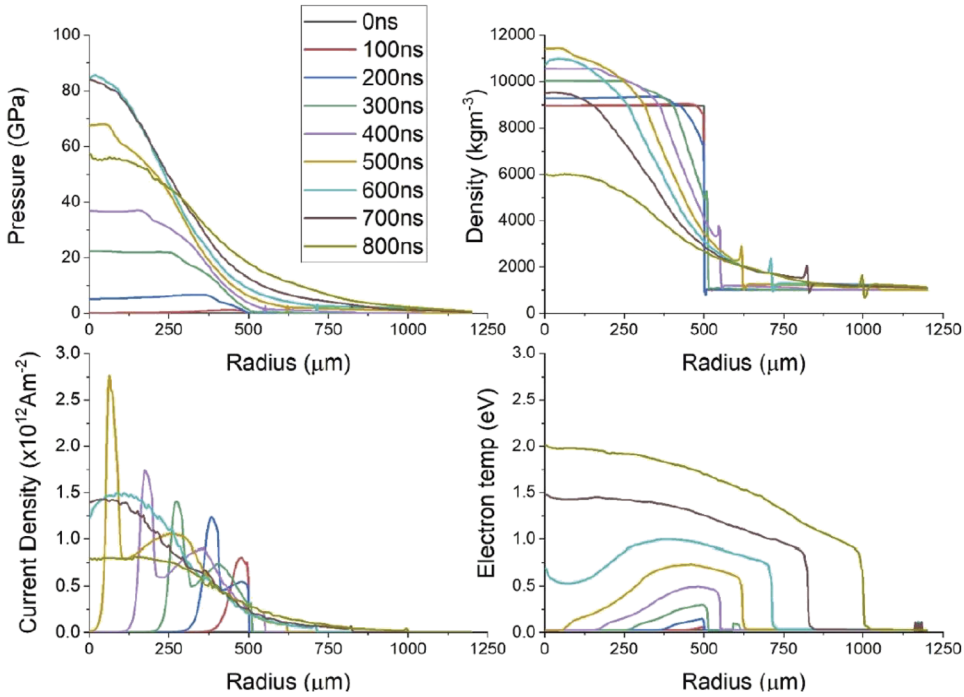

FIG. 9. Line outs of the thermal pressure, density, current density, and electron temperature, from simulations for a 1 mm Cu rod driven by 0.67 MA current peaking at 700 ns (matched to experiment).

~7 GPa. The simulations suggest the density of the copper rod peaks at ~9570 kg/m^3.

With a 1 mm rod, the dynamics are complicated by current diffusing to the axis before the peak current and expansion of the rod. The temperature of the material on the outside of the rod reaches the boiling point of copper between 300 ns and 400 ns after the start of the current, at which point copper starts to expand against water. As in the 2 mm case, the current and magnetic field diffuse into the rod with a peak in the current density corresponding to colder, metallic copper, and a tail in the hotter material behind this. At ~500 ns, significant current has still not reached the axis of the rod, and the pressure here has increased to ~70 GPa in cold material—as expected, this is significantly higher than in the 2 mm case. For comparison, the Mie Grüneisen model predicts pressures of 34 GPa. The density on axis at this point is 11 500 k/gm^3. After ~500 ns, the diffusing current reaches the axis and ohmically heats the material here, increasing the peak pressure to ~85 GPa. At this time, current is distributed over the entire volume of the rod material, heating into a warm dense state, and expansion of the rod results in the density on axis dropping to <10 000 kg/m^3 even though pressure is peaked.

In order to estimate whether or not our experiments had benefitted from the presence of water tamping the expansion of the rod and potentially increasing the peak pressure, we also ran a set of simulations with vacuum replacing water. As expected, in vacuum, the outside rod expanded faster than when the rod was in water—for instance, by 500 ns, it had reached a radius of 661 μm cf. 622 μm; however, the difference was not large, most likely as the material impedance of copper was significantly higher than water (at least initially before the water was snowploughed by the expanding copper and copper's density dropped). The rate at which current diffused through the rods was the same in both cases, and at 500 ns, the pressures on axis were similar. However, between 600 ns and 700 ns, the peak pressure on axis was surprisingly slightly higher when a vacuum was used than when the rod was surrounded with water (95 GPa vs 85 GPa). This appeared to be due to the faster expansion of the material from the rod creating a rocket effect, and more current remaining concentrated on the axis.

The simulations enable us to better interpret some of the experimental data. The current diffusing to the axis of the 1 mm diameter rod prior to the peak current and the subsequent redistribution of current into the expanding rod material can result in the rod having a lower inductance than the 2 mm diameter rod; indeed by 800 ns, the outer boundary of the rod has reached 2 mm diameter—while for the 2 mm diameter rod, any changes of inductance will happen much later in time (the diffusing current is expected to reach the axis of the 2 mm rod during/after the negative current peak). The heating of the entire volume of the 1 mm rod material in the warm dense state will result in a significantly more resistive load than in the 2 mm case, which is still partially metallic at this point. These are both consistent with the changes observed in the current waveform of the 1 mm rod compared to the 2 mm rod in Sec. III A.

The precise cause of the outflow observed in the shadowgraphy images and axial streak photographs, however, cannot be explained by these 1D calculations. Simulations predict that the pressure on the axis of both rods will reach the yield strength of copper almost as soon as the compression waves arrive on axis, ~100 ns after the start of the current pulse for the 1 mm diameter rod and ~200 ns for the 2 mm rod. However, the outflows from both rods appear to start at the same time ~500 ns, which is much later. Additionally, the outflows appear to originate from the entire width of the rod, although

the single line of sight and projection into a 2D image make it difficult to conclude whether this originates from the surface face or from the circumference of the end of the rod. The simulations predict that the surface of the 2 mm diameter rod will begin to boil >800 ns after the start of the current, whereas the 1 mm rod surface will reach the boiling point at ~300 ns—again neither agreeing with the time the outflow was observed to begin. It could be that the outflow we see at these early times is actually water, heated through thermal contact with the rod, though again this does not explain the lack of any time difference.

A more realistic possibility is the outflow is caused by current diffusing through the electrode holding the rod in place and then ablating material from around the join between the rod and electrode. The electrode is made of stainless steel, which is much more resistive than copper—hence, diffusion occurs on a faster timescale. The electrode is also of the same thickness (~1.5 mm next to the rod) in both cases and subject to similar rates of rise of current, which is consistent with the timing of the outflow seen in the 1 mm and 2 mm diameter rods.

To explore the effect of diffusion, 2D r-z calculations were performed for the 1 mm diameter rod. The spatial resolution was 5 μm. The $\sin^2$ current profile that was used for the 1D simulations was again used. Figure 10 shows initial results from these simulations.

The simulations suggest that diffusion is indeed responsible for the bubble-like shape of the outflow observed in shadowgraphy images, though its precise operation is more complicated than initially suspected. The relatively low resistivity of the copper rod compared to the stainless steel electrode means that current does not simply transfer between them at the lowest contact point as

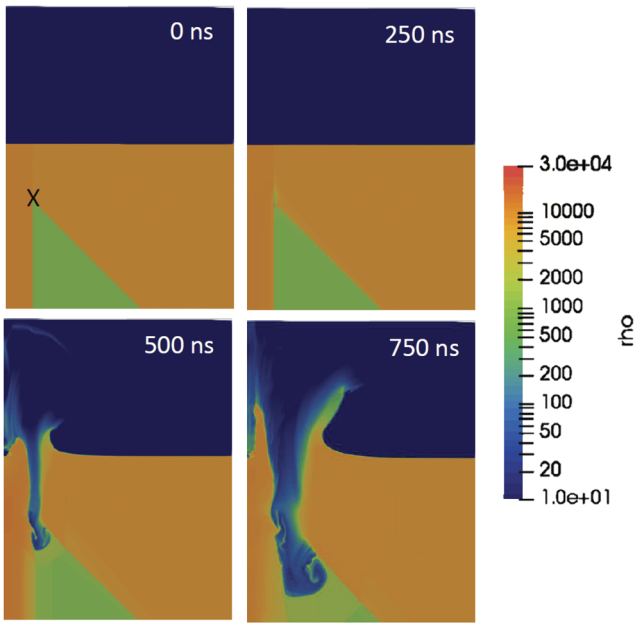

FIG. 10. 2D r-z simulations of the 1 mm diameter copper rod with stainless steel electrode driven by 630 kA peak, 800 ns rise time $\sin^2$ current pulse. The density maps are for 0 ns, 250 ns, 500 ns, and 750 ns after the start of the current flowing through the rod. Densities are in kg/m^3.

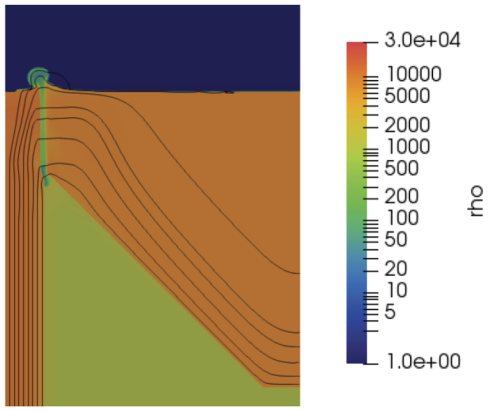

FIG. 11. Close-up density map of 2D simulations shown in Fig. 10, at t = 400 ns with current stream lines in black. Densities are in kg/m^3.

expected (marked by an X in the first frame of Fig. 10). Instead, current tends to continue to flow axially along the rod, transferring from the stainless steel over a long distance, as shown in Fig. 11, in which the current streamlines change direction suddenly along the copper–stainless steel boundary. This sets up an explosive $\mathbf{J}\times\mathbf{B}$ force around connection between the rod and the electrode, opening up a gap between them that grows from the lowest contact point, up to the surface adjacent to the air between 400 ns and 500 ns after the start of the current, the onset of which is also visible in Fig. 10.

As the gap opens up, ablated plasma—mainly stainless steel, again due to its higher resistivity—is projected above the rod as an expanding ring—resulting in the toroidal bubble-shaped outflow that was observed in the shadowgraphy images. The expansion of the bubble is driven by the $\mathbf{J}\times\mathbf{B}$ force and ∇P force in the gap continually supplying it with ablated material.

Both the timing of when this occurs and the resultant "bubble" shape above the rod are in good agreement with experimental observations; however, the dynamics of the bubble as it expands are difficult to compare quantitatively. Unlike for the experimental data shown in Fig. 6, the bubble front surface accelerates in these simulations rather than decelerating. The simulations indicate that this acceleration is due to increased material outflow from the gap providing additional ram pressure to the bubble front, as the process accelerates while current increases. In the experiment, it is likely that a breakdown occurs in this gap, causing the outflow to slow significantly and the energy of the bubble front to decay. Unfortunately, simulation of this semi-random breakdown effect is very difficult, and none of our experimental diagnostics can tell us when and how this breakdown occurred.

Only relatively late in time does slower moving, dense copper material start to move axially. The final frame of Fig. 10 shows the onset of a pinching effect around 1.5 mm down the rod, which can cause the acceleration of the top pinched-off section at later times.

V. CONCLUSIONS

Electrical explosions of 1 mm and 2 mm diameter copper rods in water baths were carried out with currents of ~0.6 MA and rise times of 700 ns–800 ns. Laser backlit shadowgraphy above the rods

showed an outflow from the end of the rod that expanded both axially and radially. The outflow began ~500 ns after the start of the current and continued throughout the experiment. Ballistics gel results suggested that the outflow contained two parts—one a low density gas/plasma, which is likely what was observed in the shadowgraphy; the other a high speed condensed projectile made of the rod material. However, the precise timing of when this projectile was launched and its speed were hidden by the plasma.

1D and 2D Gorgon simulations helped interpret the experimental results. They showed that in the case of a 1 mm diameter rod, current diffusion reached the axis of the rod just before the peak current. The entire volume of the rod was heated into a resistive warm dense state, resulting in current decaying more rapidly than in the 2 mm case. Expansion of the heated rod material and redistribution of the current also dropped the inductance of the 1 mm rod compared to the 2 mm rod during the experiment, resulting in a faster oscillating current. The simulations suggested that the outflow observed in the optical images may not have been a result of the rod heating or compression. This thought leaves the questions regarding how we could utilize the pressures predicted to be produced on axis.

As well as simulating the compression of a rod in a water bath, simulations were also performed for rods driven in vacuum to see what effect tamping of the rod's expansion may have had on the peak pressure. Surprisingly, the peak pressure in the vacuum case was predicted to be slightly greater than with water, apparently due to faster expansion of the material from the rod's surface.

Now that the Gorgon code has been tested using these experiments, it will be used to inform future designs—in particular, exploring different electrode materials and configurations, and the use of hollow and tapered rods, in 2D and 3D. Experimentally, significant improvements to diagnostics are planned including the use of better diagnostics, in particular, multi-frame hard x-ray radiography, performed either in house, or at a third generation synchrotron, to study the pressure produced internally to the rod, the movement of the ends of the rod, and the origin of the dense projectile.

ACKNOWLEDGMENTS

This research was funded by EPSRC, First Light Fusion Ltd., the U.S. Department of Energy, under Cooperative Agreement Grant Nos. DE-NA0003764 and DE-SC0018088 and Sandia National Laboratories. The authors would also like to thank Ory Schnitzer for fruitful discussions on non-linear diffusion.

DATA AVAILABILITY

The data that support the findings of this study are available from the corresponding author upon reasonable request.

REFERENCES

[1] D. B. Reisman, A. Toor, R. C. Cauble, C. A. Hall, J. R. Asay, M. D. Knudson, and M. D. Furnish, "Magnetically driven isentropic compression experiments on the Z accelerator," J. Appl. Phys. **89**, 1625 (2001).
[2] M. D. Knudson, "Megaamps, megagauss, and megabars: Using the Sandia Z Machine to perform extreme material dynamics experiments," AIP Conf. Proc. **1426**, 35 (2012).
[3] R. W. Lemke, D. H. Dolan, D. G. Dalton, J. L. Brown, K. Tomlinson, G. R. Robertson, M. D. Knudson, E. Harding, A. E. Mattsson, J. H. Carpenter, R. R. Drake, K. Cochrane, B. E. Blue, A. C. Robinson, and T. R. Mattsson, "Probing off-Hugoniot states in Ta, Cu, and Al to 1000 GPa compression with magnetically driven liner implosions," J. Appl. Phys. **119**, 015904 (2016).
[4] S. A. Slutz and R. A. Vesey, "High-gain magnetized inertial fusion," Phys. Rev. Lett. **108**, 025003 (2012).
[5] M. Weinwurm, S. N. Bland, and J. P. Chittenden, "Metal liner-driven quasi-isentropic compression of deuterium," Phys. Plasmas **20**, 092701 (2013).
[6] P. F. Knapp, M. R. Martin, D. H. Dolan, K. Cochrane, D. Dalton, J.-P. Davis, C. A. Jennings, G. P. Loisel, D. H. Romero, I. C. Smith, E. P. Yu, M. R. Weis, T. R. Mattsson, R. D. McBride, K. Peterson, J. Schwarz, and D. B. Sinars, "Direct measurement of the inertial confinement time in a magnetically driven implosion," Phys. Plasmas **24**, 042708 (2017).
[7] D. Hayes, "Introduction to stress wave phenomena," Sandia Labs Report SLA-73-0801, 1973.
[8] O. Schnitzer, "Fast penetration of megagauss fields into metallic conductors," Phys. Plasmas **21**, 082306 (2014).
[9] S. Fuelling, T. J. Awe, B. S. Bauer, T. Goodrich, A. Haboub, V. V. Ivanov, V. Makhin, A. Oxner, R. Presura, and R. E. Siemon, "A Zebra experiment to study plasma formation by megagauss fields," IEEE Trans. Plasma Sci. **36**, 62 (2008).
[10] S. Pikuz, T. Shelkovenko, V. Romanova, D. Sinars, D. Hammer, S. Bland, and S. Lebedev, "X pinch as a source for x-ray radiography," Nukleonika **46**, 21–25 (2001).
[11] O. T. Strand, D. R. Goosman, C. Martinez, T. L. Whitworth, and W. W. Kuhlow, "Compact system for high-speed velocimetry using heterodyne techniques," Rev. Sci. Instrum. **77**, 083108 (2006).
[12] M. A. Kadatskiy and K. V. Khishchenko, "Theoretical investigation of the shock compressibility of copper in the average-atom approximation," Phys. Plasmas **25**, 112701 (2018).
[13] M. F. Ashby, *Materials Selection in Mechanical Design* (Butterworth-Heinemann, Oxford, 2005).
[14] B. R. Munson, D. F. Young, T. H. Okiishi, and W. W. Huebsch, *Fundamentals of Fluid Mechanics* (Wiley, 2009).
[15] J. P. Chittenden, S. V. Lebedev, C. A. Jennings, S. N. Bland, and A. Ciardi, "X-ray generation mechanisms in three-dimensional simulations of wire array Z-pinches," Plasma Phys. Controlled Fusion **46**, B457 (2004).
[16] J. D. Pecover and J. P. Chittenden, "Instability growth for magnetized liner inertial fusion seeded by electro-thermal, electro-choric, and material strength effects," Phys. Plasmas **22**, 102701 (2015).
[17] M. P. Desjarlais, J. D. Kress, and L. A. Collins, "Electrical conductivity for warm, dense aluminum plasmas and liquids," Phys. Rev. E **66**, 025401 (2002).
[18] G. R. Johnson and W. H. Cook, "Fracture characteristics of three metals subjected to various strains, strain rates, temperatures and pressures," Eng. Fract. Mech. **21**, 31 (1985).
[19] S. Faik, A. Tauschwitz, and I. Iosilevskiy, "The equation of state package FEOS for high energy density matter," Comput. Phys. Commun. **227**, 117 (2018).